PERGAMON

International Journal of Heat and Mass Transfer 45 (2002) 4577–4587

International Journal of HEAT and MASS TRANSFER

www.elsevier.com/locate/ijhmt

Linear stability analysis of the solidification of a supercooled liquid in a half-space

R.A. Lambert, R.H. Rangel *

Department of Mechanical and Aerospace Engineering, University of California, Irvine, CA 92697-3975, USA

Received 15 March 2002; received in revised form 29 April 2002

Abstract

The instability of the solidifying front of a supercooled liquid in a half-space is investigated by introducing a small disturbance at the solid–liquid interface. A relationship between the thermal properties of the material and the disturbance growth rate is obtained using the heat balance equation at the interface, including the effects of surface curvature on the equilibrium temperature. The heat balance equation is solved numerically and compared to the analytical solution obtained by neglecting the effects of surface curvature. The results show that the thermal gradients increase the growth rates of disturbances at the solid–liquid interface and that the effect of surface curvature results in a decrease in the disturbance growth rates. Further analysis shows that marginal stability occurs in both the longer wavelength and capillary regions.

1. Introduction

The instability of a solidifying front can lead to the appearance of dendrites and cellular structures within a solidifying material. This phenomenon has important implications in the field of materials science, relating in particular to processing of alloys and homogeneous substances since the nature of the solidification process directly relates to the quality of the final product obtained. For a solidifying front in a half-space, previous investigations have shown that crystal formation can be predicted by the growth of a disturbance introduced along the solid–liquid interface. Perturbation analyses have been applied to solidification problems and correlate the stability of a solidifying interface with the appearance of cellular growth [1–5].

In this study, we conduct a linear stability analysis of the modified Stefan problem for a thermally supercooled, homogeneous material. The undisturbed problem is a classical phase-change problem of solidification in a half-space [6]. The purpose of this investigation is to relate the effects of thermal supercooling and surface curvature on the growth of linear disturbances under unsteady thermal conditions. The unsteady energy equations are solved using a similarity variable and assuming that the densities in the liquid and solid phases are equal and constant. We conduct a linear stability analysis by regular perturbation of the thermal energy equation where only first-order terms are retained. As an indication of stability, only positive values of the wave number are considered physically relevant in the analysis. This analysis neglects solute diffusion found in multicomponent solidification, which has been the primary focus of continuing investigations. By focusing on a homogeneous material, this analysis provides insight into the solidification of a planar front that advances at a rate proportional to $t^{-1/2}$. Stagnant conditions exist in the fluid and convection does not occur.

In linear perturbation analysis, an arbitrary disturbance along a planar interface can be represented by a summation of modal disturbances of varying wavelength and negligible amplitude. A condition for linear stability analysis is that the amplitude of the disturbance be negligible in comparison to the characteristic lengths of the posed problem. The application of linear disturbance analysis in solidification problems was first introduced by Mullins and Sekerka [1] to a steady-state

* Corresponding author. Tel.: +1-949-824-4033; fax: +1-949-824-8585.

E-mail address: rhrangel@uci.edu (R.H. Rangel).

0017-9310/02/$ - see front matter
PII: S0017-9310(02)00166-7

Nomenclature

c_p	specific heat of constant pressure, J/kg K
d_0	capillary length, m
f	marginal stability function
g	thermal function
h	capillary function
h_{sf}	specific latent heat of fusion, J/kg
K	surface curvature, m^{-1}
k	wave number, $2\pi/\lambda_0$
$\hat{k}$	dimensionless wave number, $k\sqrt{\alpha_l \tau}$
Ste_0	background Stefan number, $c_p(T_m - T_i)/h_{sf}$
s	thickness of the solid phase, m
T	phase temperature, K
T_i	temperature of the supercooled liquid, K
T_m	melting temperature, K
t	time, s
x	distance along the x-axis, m
y	distance along the y-axis, m

Greek symbols

α	thermal diffusivity, m^2/s
β_l	parameter, $\sqrt{k^2 - (i\omega/\alpha_l)}$
β_s	parameter, $\sqrt{k^2 - (i\omega/\alpha_s)}$
B	dimensionless capillary number
Γ	Gibbs–Thompson coefficient, m K
ε	disturbance amplitude at the interface, m
κ	thermal conductivity
λ	dimensionless solidification parameter
λ_0	disturbance wavelength
ρ	density in the solid and liquid phase
σ	interfacial energy, J/kg
τ	time at which disturbance is applied, s
ϕ	amplitude equation of the temperature disturbance, K
Ω	disturbance growth rate, s^{-1}
$\hat{\Omega}$	dimensionless growth rate, $\Omega\tau$
ω	wavelength frequency, s^{-1}

Subscripts

l	liquid phase
0	background or undisturbed region
s	solid phase

Superscript

$'$	disturbance

problem involving constitutional undercooling, the effect of mass transport on thermal equilibrium in alloys. In addition to constitutional undercooling, Mullins and Sekerka identified an additional factor influencing interface stability, the undercooling at the liquid interface due to the surface curvature.

The curvature of a disturbance begins to have an effect on the local phase-change temperature when the radius of curvature is very small, on the order of 10 μm [4]. The effect that the curvature has on the melting temperature is called the undercooling effect or the capillary effect since the surface curvature is very large at smaller wavelengths. Following thermodynamic principles, a large convex curvature at the interface as seen from the liquid side, can be described mathematically as the result of a high pressure in the solid region, on the order of 100 MPa, created by the high interfacial energy [4]. The high pressure in the solid further lowers the free energy at the surface, thereby reducing the equilibrium temperature at which the material solidifies. In this study we assume that the interfacial energy is constant and isotropic. Anisotropy becomes an important consideration in the predictions of shapes and growth formations of dendrites and cells. Similarly, the effects of nucleation kinetics on surface temperature and stability are neglected.

In the analysis of the constitutionally undercooled problem in a steady-state thermal field, Mullins and Sekerka [1] conclude that positive values of the disturbance growth rate cause instability at the interface, while negative values lead to disturbance decay. In the steady-state problem, the solid–liquid interface advances at a constant rate. Solutions of this problem [1,2] show that the effects of surface curvature and positive thermal gradients at the interface increase stability at the solid–liquid interface, while negative thermal gradients produce instability at the interface. In the longer wavelength region, stability is dominated by positive thermal gradients in the liquid and the capillary effect dominates stability after a critical wave number in the capillary region. Mullins and Sekerka identified a range of intermediate wavelengths that are unstable. In an unsteady diffusion problem, Delves [5,7] and Sekerka [8] show that when the growth rate has an imaginary component, the disturbance at the interface is always stable. Positive values of the growth rate with non-zero imaginary components do not occur. The findings show that the interface does not support undamped oscillatory motion.

One of the limitations of the linear stability analysis is that the condition of stability does not determine final cell size or the morphology [1,4]. For similarity solutions of the unsteady mass diffusion problem, Sekerka [8] concludes that proportionality with half power in time is an oversimplification of the solidification process, since the velocity of the solidification front will approach in-

finity as time approaches zero. The linear kinetic law explains the behavior of the advancing front for initial time values and is relevant to times on the order 10^{-8} [9]. The proportionality of the advancement of the solidifying front with half powers in time will not change the condition of stability in this analysis, therefore the similarity variable defined in this analysis will be used. Sekerka [8] also concludes that the time dependence of the advancement of the solidifying front changes how the stability of the interface evolves in time. As time evolves, the perturbations become too large for linear theory to be valid. For the purposes of this analysis we apply the linear analysis to the point at which the planar surface becomes unstable and do not analyze the growth of the disturbance in time.

Experimentally, the growth of dendrites and cell structures in a solidifying front has been shown to have greater complexity than that predicted by linear perturbation theory. Under solidifying conditions, other imperfections such as grain boundaries and foreign particles play a role in the development of interfacial growth [10]. Experimental results under controlled conditions have been found to be in quantitative agreement with the perturbation theory applied to the solidification of multi-component substances [10–12].

2. Mathematical formulation

In this problem, we consider a supercooled liquid with temperature T_i that is in contact with a flat surface of infinite dimensions at the liquid melting temperature T_m. Initial nucleation along the surface of a wall causes the liquid in contact with the wall to solidify. The liquid continues to solidify along a moving solidification front so that the solid thickness is $s(t)$. This is a classical phase change problem known as the modified Stefan problem, with a solution postulated by Neumann using similarity methods [6]. We consider the time evolution of a disturbance $s'(y,t)$ introduced at an arbitrary time, t, superimposed on the undisturbed front with thickness $s_0(t)$ as shown in Fig. 1.

The undisturbed thickness of the solid region is [6]

$$s_0(t) = 2\lambda\sqrt{\alpha_l t}, \tag{1}$$

where the solidification parameter, λ, is a constant of proportionality between a characteristic solidification length, s_0, to a thermal diffusion length, $\sqrt{\alpha_l t}$. For conditions in which a surface disturbance with small amplitude is introduced, the undisturbed thickness of the solid region represents a characteristic length for arbitrary values of time. The solidification parameter is related to constants of proportionality used in other works. For spherical growth under steady-state conditions, a Peclet number, similar in function to the solidification parameter, used in the Ivanstov solution has been identified [13]. High values of the solidification parameter indicate rapid solidification within the material.

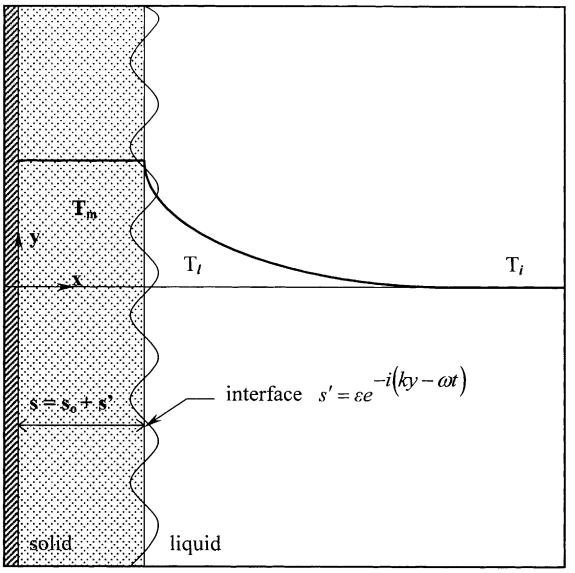

Fig. 1. Solidification of a supercooled liquid in a half-space with an initial disturbance at the solid–liquid interface.

The Neumann solution relating the solidification parameter, λ, and the Stefan number yields [6]

$$\lambda \operatorname{erfc}\lambda e^{\lambda^2} = \frac{Ste_0}{\sqrt{\pi}}, \tag{2}$$

where Ste_0 is the background Stefan number which can also be viewed as a measure of thermal supercooling.

Neglecting the effects of curvature, the relationship between the background thermal supercooling and the solidification parameter is shown by the solid line in Fig. 2. No solution exists for a background Stefan number equal or greater than 1. At a Stefan number greater than 1, instantaneous freezing of the liquid would occur. Experiments of crystallization in solidifying materials show that the measured Stefan number of the perturbations along an interface is higher than the Stefan number for a planar interface [13]. In this analysis, the Stefan number is calculated for thermal supercooling and includes the additional undercooling resulting from linear perturbations at the surface

$$Ste = Ste_0 + d_0 K, \tag{3}$$

where K is the surface curvature

$$K = \frac{\frac{\partial^2 s'}{\partial y^2}}{\left(1 + \left(\frac{\partial s'}{\partial y}\right)^2\right)^{3/2}} \approx \frac{\partial^2 s'}{\partial y^2}, \tag{4}$$

since the disturbance is very small.

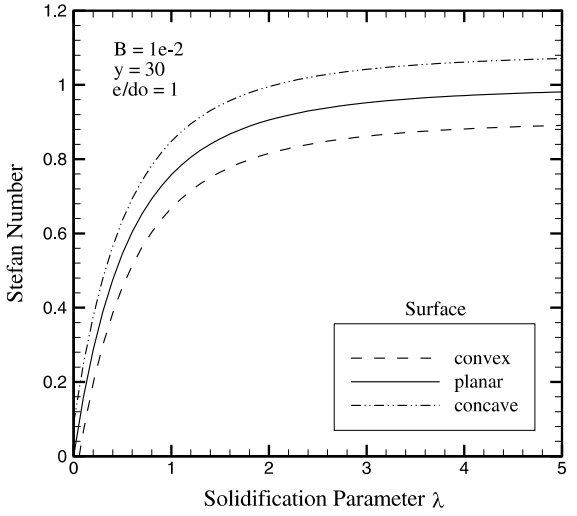

Fig. 2. Relationship between the Stefan number at the solid–liquid interface and the solidification parameter λ.

A capillary length, d_0, is defined in this analysis as

$$d_0 = \frac{c_p \Gamma}{h_{sf}}, \tag{5}$$

where Γ is a capillary constant called the Gibbs–Thompson coefficient [4] defined by the interfacial energy, σ, and the specific latent heat of solidification, h_{sf}, as

$$\Gamma = \frac{T_m \sigma}{\rho h_{sf}}. \tag{6}$$

The capillary number, B, is a dimensionless constant of proportionality between the capillary length and the thermal diffusion length

$$B = \frac{d_0}{\sqrt{\alpha_l t}}. \tag{7}$$

Terms that relate the capillary length to thermal properties of a solidifying material have been used in previous works and are referred to as the selection parameter [14] and the dimensionless velocity of solidification [2].

3. Unsteady energy equation

The geometry of solidification on a flat surface is reduced to two dimensions. Employing modal analysis, the location of the disturbed front is

$$s(t) = s_0(t) + s'(y,t) = 2\lambda\sqrt{\alpha_l t} + \varepsilon e^{i(ky-\omega t)}, \tag{8}$$

where a prime denotes the disturbance.

The temperature of the liquid is

$$T_l = T_{l0}(x,t) + T_l'(x,y,t), \tag{9}$$

and the temperature of the undisturbed liquid, T_{l0}, is the solution to the one-dimensional conduction equation that satisfies the following boundary conditions: $T_{l0} = T_i$ at a distance far away from the interface and $T_{l0} = T_m$ at the interface. Thus, the equations for the undisturbed temperature and for the temperature disturbance are [6]

$$\frac{(T_{l0} - T_i)}{(T_m - T_i)} = \frac{\operatorname{erfc}\left(\frac{x}{2\sqrt{\alpha_l t}}\right)}{\operatorname{erfc}\lambda}, \quad T_l' = \phi_l(x) e^{i(ky-\omega t)}. \tag{10}$$

Similarly, in the solid region,

$$T_s = T_{s0} + T_s'(x,y,t), \tag{11}$$

where the undisturbed solid phase temperature, T_{s0}, is constant and the disturbance temperature is

$$T_s' = \phi_s(x) e^{i(ky-\omega t)}. \tag{12}$$

The unsteady energy equations of the disturbance in the liquid and solid phases are

$$\frac{\partial T_s'}{\partial t} = \alpha_s\left(\frac{\partial^2 T_s'}{\partial x^2} + \frac{\partial^2 T_s'}{\partial y^2}\right), \quad \frac{\partial T_l'}{\partial t} = \alpha_l\left(\frac{\partial^2 T_l'}{\partial x^2} + \frac{\partial^2 T_l'}{\partial y^2}\right). \tag{13}$$

By substituting Eqs. (10) and (12) into Eq. (13), the linear diffusion equations are transformed into the following system of equations in terms of the amplitude of the temperature disturbance

$$\ddot{\phi}_s - \left(k^2 - \frac{i\omega}{\alpha_s}\right)\phi_s = 0, \quad \ddot{\phi}_l - \left(k^2 - \frac{i\omega}{\alpha_l}\right)\phi_l = 0. \tag{14}$$

These equations are solved using the boundary conditions defined at the wall, the solid–liquid interface, and at a distance far away from the interface. Eqs. (10) and (12) contain the assumption that the ϕ_l and ϕ_s functions are independent of time. This is an approximation, which becomes exact in the limit of a slowly varying background solution. The fact that the background solution is time-dependent constitutes the temporal analogy to the non-parallel problems that arise in studies of interface instability in the spatial development of shear layers. Assuming time-independence of the ϕ_s and ϕ_l functions is equivalent to making a frozen-field assumption of the background flow, meaning that the disturbance growth is examined as superimposed on the frozen background field that exists at any given time.

At the solid–liquid interface, the temperature of the solid and liquid are equal. The equations for the temperature at the interface in the liquid and solid phase at $x = s_0 + s'$, including the capillary correction, are [4]:

$$T_{s0} + T_s' = T_m + \Gamma K, \quad T_{l0} + T_l' = T_m + \Gamma K, \tag{15}$$

where K is the surface curvature.

A Taylor-series expansion of Eq. (15) about the undisturbed interface, s_0, leads to a set of equations with reduced variables, that can be expressed in terms of the amplitude of the temperature disturbance

$$T_{s0}|_{s0} + s' \left.\frac{\partial T_{s0}}{\partial x}\right|_{s0} + T'_s|_{s0} + s' \left.\frac{\partial T'_s}{\partial x}\right|_{s0} + \text{h.o.t.} = T_m + \Gamma K. \tag{16}$$

Retaining only first-order terms, Eq. (16) reduces to

$$T'_s|_{s0} = \Gamma \frac{\partial^2 s'}{\partial y^2}. \tag{17}$$

Eq. (17) is rewritten in terms of Eqs. (8) and (12), and represents the boundary condition at the solid–liquid interface in the solid region

$$\phi_s(s_0) = -\varepsilon \Gamma k^2. \tag{18}$$

Similarly, in the liquid, a Taylor-series expansion about the undisturbed interface s_0 in Eq. (15), results in the following relationship

$$T_{l0}|_{s0} + s' \left.\frac{\partial T_{l0}}{\partial x}\right|_{s0} + T'_l|_{s0} + s' \left.\frac{\partial T'_l}{\partial x}\right|_{s0} + \text{h.o.t.} = T_m + \Gamma K, \tag{19}$$

which reduces to

$$T'_l|_{s0} = -s' \left.\frac{\partial T_{l0}}{\partial x}\right|_{s0} + \Gamma \frac{\partial^2 s'}{\partial y^2}, \tag{20}$$

upon retaining only linear terms. Eq. (20) is rewritten in terms of Eqs. (8) and (10)

$$\phi_l(s_0) = \frac{\varepsilon (T_m - T_i)}{\sqrt{\pi \alpha_l t}} \frac{e^{-\lambda^2}}{\operatorname{erfc} \lambda} - \varepsilon \Gamma k^2 \tag{21}$$

and represents the boundary condition at the interface in the liquid phase.

At the wall, the disturbance vanishes, thus:

$$T'_s(0) = 0, \quad \phi_s(0) = 0. \tag{22}$$

Far from the wall, as x approaches infinity, the effect of the disturbance on the liquid temperature approaches zero:

$$T'_l(\infty) = 0, \quad \phi_l(\infty) = 0. \tag{23}$$

3.1. Solution of the perturbation equations

Using the boundary conditions defined in Eqs. (18) and (22), the solution to the energy equation (14) in the solid phase is

$$\phi_s(x) = -\varepsilon \Gamma k^2 \frac{\sinh(\beta_s x)}{\sinh(\beta_s s_0)} \tag{24}$$

The solution to the energy equation (14) in the liquid phase for the boundary conditions defined in Eqs. (21) and (23) is

$$\phi_l(x) = \varepsilon \left[\frac{(T_m - T_i)}{\sqrt{\pi \alpha_l t}} \frac{e^{-\lambda^2}}{\operatorname{erfc} \lambda} - \Gamma k^2 \right] e^{\beta_l (s_0 - x)}. \tag{25}$$

Eqs. (24) and (25) show that the amplitudes of the temperature disturbance, ϕ_s and ϕ_l, defined in the modal analysis, are functions of time as explained earlier. In the following section, the stability of the disturbance at a fixed time $t = \tau$ is analyzed. The disturbance can be unstable when the frequency, ω, is complex. When ω is positive and complex, the amplitude of the disturbance grows exponentially. When ω is negative and imaginary, the disturbance decays and the front remains planar. Real values of the frequency represent a traveling wave component, which is either damped or un-damped. The results show that the interface will not support an un-damped traveling wave.

4. Dispersion analysis

The relationship between the dimensionless growth rate and wave number can be analyzed using an energy balance across the solid–liquid interface. At $x = s$,

$$\rho h_{sf} \frac{\partial s}{\partial t} = \kappa_s \frac{\partial T_s}{\partial x} - \kappa_l \frac{\partial T_l}{\partial x}, \tag{26}$$

or

$$\rho h_{sf} \frac{\partial}{\partial t}(s_0 + s') = \kappa_s \frac{\partial}{\partial x}(T_{s0} + T'_s) - \kappa_l \frac{\partial}{\partial x}(T_{l0} + T'_l). \tag{27}$$

A Taylor-series expansion about s_0, neglecting higher order terms, leads to

$$\rho h_{sf} \frac{\partial}{\partial t}(s_0 + s') = \kappa_s \left.\frac{\partial T'_s}{\partial x}\right|_{s0} - \kappa_l \left(\frac{\partial T_{l0}}{\partial x} + s' \frac{\partial^2 T_{l0}}{\partial x^2} + \frac{\partial T'_l}{\partial x} \right)\Bigg|_{s0}, \tag{28}$$

or, after the terms for the temperature gradient in the undisturbed temperature field are removed

$$\rho h_{sf} \frac{\partial s'}{\partial t} = \kappa_s \left.\frac{\partial T'_s}{\partial x}\right|_{s0} - \kappa_l s' \left.\frac{\partial^2 T_{l0}}{\partial x^2}\right|_{s0} - \kappa_l \left.\frac{\partial T'_l}{\partial x}\right|_{s0}. \tag{29}$$

Eq. (29) can be expressed in terms of the disturbance amplitude in the thermal field by substituting Eqs. (8), (10) and (12) as follows

$$-\varepsilon i \omega \rho h_{sf} = \kappa_s \dot{\phi}_s(s_0) - \frac{\varepsilon \kappa_l \lambda (T_m - T_i)}{\alpha_l \tau \sqrt{\pi} \operatorname{erfc} \lambda} e^{-\lambda^2} - \kappa_l \dot{\phi}_l(s_0). \tag{30}$$

From the solutions to the energy equations, as described in Eqs. (24) and (25), the amplitude of the temperature disturbance in the solid phase at s_0 is

$$\dot{\phi}_s(s_0) = -\varepsilon\beta_s \Gamma k^2 \coth(\beta_s s_0), \tag{31}$$

while in the liquid phase it is

$$\dot{\phi}_l(s_0) = -\varepsilon\beta_l \left(\frac{(T_m - T_i)e^{-\lambda^2}}{\sqrt{\pi\alpha_l\tau}\,\mathrm{erfc}\,\lambda} - \Gamma k^2 \right). \tag{32}$$

By making the substitution $\omega = i\Omega$, and introducing the background Stefan number Ste_0 and the capillary number B, Eq. (30) is rewritten in dimensionless form as

$$\begin{aligned}\Omega\tau = {} & -Bk^2\alpha_l\tau\sqrt{k^2\alpha_l\tau + \frac{\alpha_l}{\alpha_s}\Omega\tau} \\ & \times \left(\frac{k_s}{k_l}\coth\left(2\lambda\sqrt{k^2\alpha_l\tau + \frac{\alpha_l}{\alpha_s}\Omega\tau}\right) + 1 \right) \\ & + \frac{Ste_0 e^{-\lambda^2}}{\sqrt{\pi}\,\mathrm{erfc}\,\lambda}\left(\sqrt{k^2\alpha_l\tau + \Omega\tau} - \lambda\right).\end{aligned} \tag{33}$$

Using the relationship between the background Stefan number and the solidification parameter in Eq. (2), and introducing the dimensionless growth rate $\hat{\Omega}$ and wave number $\hat{k}$ the dispersion relation becomes

$$\begin{aligned}\hat{\Omega} = {} & \lambda\sqrt{\hat{k}^2 + \hat{\Omega}} - \lambda^2 - B\hat{k}^2\sqrt{\hat{k}^2 + \frac{\alpha_l}{\alpha_s}\hat{\Omega}} \\ & \times \left(\frac{k_s}{k_l}\coth\left(2\lambda\sqrt{\hat{k}^2 + \frac{\alpha_l}{\alpha_s}\hat{\Omega}}\right) + 1 \right),\end{aligned} \tag{34}$$

which can be solved numerically for values of the dimensionless growth rate. Further assumptions are needed in order to solve Eq. (34) analytically. Analysis of a similarly posed steady-state problem that includes mass diffusion at the interface shows that a disturbance will not grow if the growth rate lags behind negative transient components in the dispersion relation [1]. We predict that negative transient components in Eq. (34) will therefore favor interface stability. The second term on the right hand side (RHS) of the equation, $-\lambda^2$, originates from the heat transfer into the undisturbed liquid temperature field and is a negative constant that has a limited effect on the stability of the interface. This implies that the stabilizing effect of the thermal gradient in the undisturbed liquid field only results in an initial shift toward stability in the longer wavelength region and does not have an added effect as the wave number increases. The third term on the RHS of Eq. (34) originates from effect of surface curvature. The capillary number, B, increases as the wavelength decreases implying that the effect of surface curvature will increase the tendency toward stability as the wave number increases.

An analytical solution of the dispersion relation is possible when the capillary effects are neglected. This reduced analytical solution provides insight into the interface stability for long wavelengths. In a perturbation analysis of a steady-state solidification problem, Sekerka and Mullins [1] found that in the longer wavelength regions, the effect of capillarity on stability is minimal until the wave numbers reach a critical value in the intermediate wavelength region. The effect of surface curvature on interface stability is further investigated by comparing the solution of the reduced analytical solution to numerical solution, which includes surface curvature effects.

5. Analytical solution

By neglecting the capillary effect, the growth rate can be obtained explicitly. The dispersion relationship at the interface neglecting curvature effects is

$$\hat{\Omega} = \lambda(\sqrt{\hat{k}^2 + \hat{\Omega}} - \lambda). \tag{35}$$

Solving Eq. (35), the dimensionless growth rate can be expressed in terms of real and imaginary components

$$\hat{\Omega} = -\frac{\lambda^2}{2}\left(1 \pm i\sqrt{3 - 4\frac{\hat{k}^2}{\lambda^2}}\right). \tag{36}$$

Eq. (36) reveals that two roots for each value of the wave number are possible. For wavelengths in the unstable regions, the roots are positive real numbers without imaginary components. This confirms findings for similarly posed problems, that the growth rate does not contain undamped traveling wave components [5,7]. Under stable conditions, the negative values for the dimensionless growth rate can have both real and imaginary components indicating that the traveling waves that appear on the surface are damped. Damped traveling waves occur in the longer wavelength region when the relationship between the dimensionless wave number and the solidification parameter is

$$\hat{k}^2 < \frac{3}{4}\lambda^2. \tag{37}$$

A critical wave number for marginal stability is found by solving Eq. (35) for real positive values of the dimensionless growth rate. Neglecting the effects of curvature, one critical wave number is found in the longer wavelength region and is related to the solidification parameter as

$$\hat{k}_c = \lambda. \tag{38}$$

This value for the critical wave number represents marginal stability in the longer wavelength region and arises from the negative temperature gradient in the undisturbed liquid phase. Wavelengths, which are longer

than the critical wavelength, are stable. Wavelengths in the intermediate and capillary regions remain unstable unless the effect of surface curvature is considered.

6. Numerical solution

Critical values for the dimensionless wave number, an indication of marginal stability can be found by solving for the roots in Eq. (34)

$$0 = \lambda\hat{k} - \lambda^2 - B\hat{k}^3\left(\frac{k_s}{k_l}\coth(2\lambda\hat{k}) + 1\right). \tag{39}$$

The roots are obtained numerically using the Newton-Raphson method [15]. Eq. (34) yields two positive values of the critical wave number, defining a range of intermediate wavelengths that result in unstable perturbations at the solid–liquid interface. The wavelengths that lie outside the range of intermediate wavelengths, when introduced on the solid–liquid interface will not grow.

7. Results

To illustrate the results, properties for aluminum were used in the numerical analysis. The values for these properties are shown in Table 1 [4]. The results of the numerical analysis show that the tendency toward instability of the solidifying front increases with increasing values of the solidification parameter. Fig. 3 shows the dispersion relation for different values of the solidification parameter, λ, when the capillary number, B, is 10^{-2} (Fig. 3a) and 10^{-3} (Fig. 3b). The curves in the figures represent wavelength regions in which the growth rate is positive and therefore the solid–liquid interface becomes unstable. Wavelengths that are outside of the region bounded by the curve are stable. Fig. 3a shows that the disturbance growth rate increases as the solidification parameter increases. Similarly, increases in the solidification parameter result in a range of unstable wavelengths that move further into the capillary region. In the longer wavelength region, increases in the solidification parameter result in an increase in stability. The behavior of the dispersion relation in the long wavelength region is illustrated in Fig. 3b for a larger capillary number. In this region, an increase in the solidification parameter will shift the point of marginal stability further into the intermediate wavelength region. The influence of the increase in the solidification parameter on stability is isolated to the longer wavelength region and does not have an added effect in the intermediate wavelength region. While an increase in the solidification parameter increases stability in the longer wavelength region, the rate of instability increases along with the range of unstable wavelengths as the wave number approaches infinity.

Values for the critical wave numbers for changes in the solidification parameter are given in Table 2. The

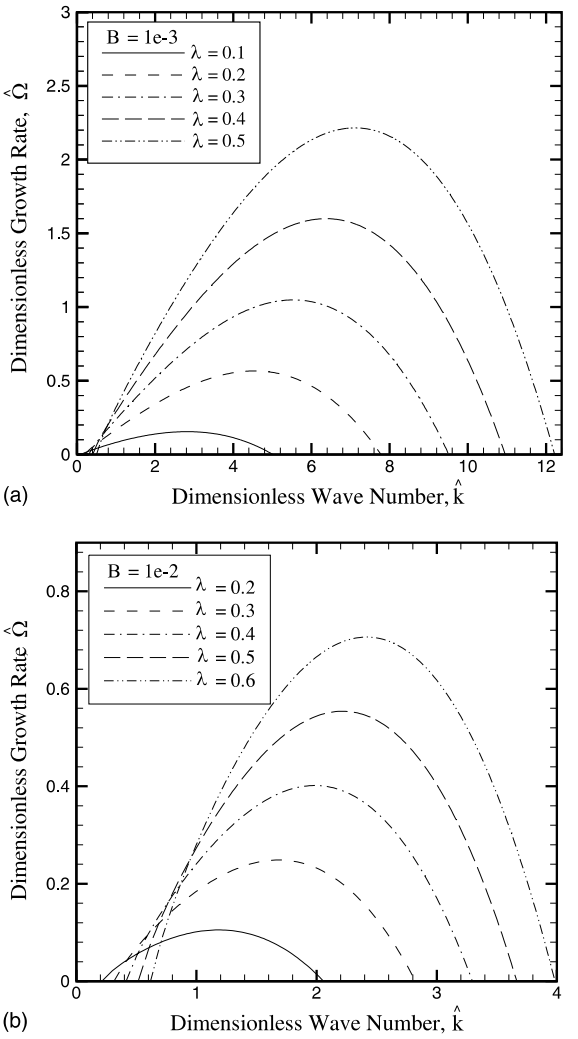

Fig. 3. Dimensionless growth rate, $\hat{\Omega}$, versus dimensionless wave number $\hat{k}$ for different values of (a) $B = 10^{-3}$, (b) $B = 10^{-2}$.

Table 1
Properties of pure Aluminum

Variable	Value	Units
c_p	1074	J/kg K
Γ	9.0×10^{-8}	K m
h_{sf}	397 490	J/kg
α_l	3.7×10^{-5}	m^2/s
α_s	7.0×10^{-5}	m^2/s
k_l	95	W/Km
k_s	210	W/Km

Table 2
Critical wave numbers as functions of the solidification parameter

λ	Critical value 1	Critical value 2	Effect of curvature on CV1
$B = 1 \times 10^{-3}$			
0.05	0.05	2.0	1.2×10^{-3}
0.1	0.1	5.0	1.1×10^{-3}
0.2	0.2	7.8	1.2×10^{-3}
0.3	0.3	9.5	1.2×10^{-3}
0.4	0.4	11.0	1.3×10^{-3}
0.5	0.5	12.2	1.5×10^{-3}
$B = 1 \times 10^{-2}$			
0.1	0.11	0.73	1.5×10^{-2}
0.2	0.21	2.06	1.3×10^{-2}
0.3	0.31	2.82	1.3×10^{-2}
0.4	0.41	3.30	1.4×10^{-2}
0.5	0.52	3.67	1.6×10^{-2}
0.6	0.62	3.98	1.8×10^{-2}

contribution of the surface curvature to the condition of marginal stability in the longer wavelength region is included. The results in the table show that as the solidification parameter increases, the effect of curvature decreases and has very slight influence on the critical wavelength in that region. The second critical wave number is the result of the capillary number. Wavelengths smaller than this value have an interfacial energy strong enough that a disturbance of this order of magnitude will not grow.

The opposite effect on surface stability is observed for increasing values of the capillary number. As the capillary number increases, the tendency toward instability decreases. Fig. 4 shows the dispersion relation for different values of the capillary number, B, when the solidification parameter, λ, is 0.05 (Fig. 4a) and 0.4 (Fig. 4b). The curves define a range of wavelengths that will result in an unstable solid–liquid interface. The results show that changes in the capillary number have a negligible effect on marginal stability in the longer wavelength region. As capillary number increases, the point of marginal stability in the capillary region shifts toward the intermediate wavelength region and the magnitude of the growth rate decreases. Ultimately, as the capillary number continues to increase, a point of unconditional stability is reached where a disturbance of any wavelength introduced at the solid–liquid interface will not grow.

The values of the critical wave numbers for changes in the capillary number, B, are given in Table 3. The results show that for increasing values of the capillary number, the effect on marginal stability in the longer wavelength region increases and shifts the critical point toward the intermediate wavelength region. The capillary number shifts the point of marginal stability toward

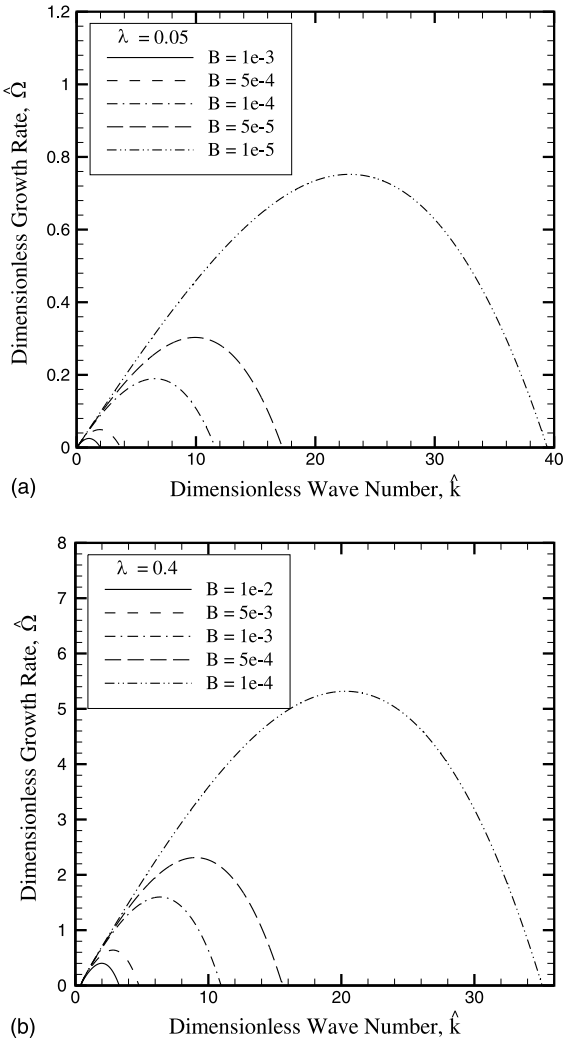

Fig. 4. Dependence of the dimensionless growth rate, $\hat{\Omega}$, on the capillary number, B, for (a) small thermal supercooling, $\lambda = 0.05$, (b) large thermal supercooling, $\lambda = 0.4$.

the intermediate region, and will eventually create the condition of absolute stability.

8. Discussion

The behavior of the transient terms on surface stability is further illustrated using certain mathematical relationships. In order to determine the nature of the effects of the temperature gradients and interfacial energy on interface stability, Eq. (34) can be expressed as the sum of two functions g and h,

$$\hat{\Omega} = g(\hat{\Omega}, \hat{k}) + h(\hat{\Omega}, \hat{k}), \tag{40}$$

Table 3
Critical wave numbers as functions of the capillary number

B	Critical value 1	Critical value 2	Effect of curvature on CV1
$\lambda = 0.4$			
5×10^{-2}	0.51	1.12	1×10^{-1}
1×10^{-2}	0.41	3.30	1×10^{-2}
5×10^{-3}	0.41	4.78	7×10^{-3}
1×10^{-3}	0.40	11.0	1×10^{-3}
5×10^{-4}	0.40	15.6	7×10^{-4}
1×10^{-4}	0.40	35.1	1×10^{-4}
$\lambda = 0.05$			
5×10^{-3}	5.7×10^{-2}	0.39	7×10^{-3}
1×10^{-3}	5.1×10^{-2}	2.0	1×10^{-3}
5×10^{-4}	5.1×10^{-2}	3.7	6×10^{-4}
1×10^{-4}	5.0×10^{-2}	11.6	1×10^{-4}
5×10^{-5}	5.0×10^{-2}	17.2	6×10^{-5}
1×10^{-5}	5.0×10^{-2}	39.4	1×10^{-5}

representing the effects of thermal gradients and the added undercooling effects of surface curvature. In the analysis we consider a function for the thermal gradients in the liquid phase

$$g(\hat{\Omega},\hat{k}) = \lambda\left(\sqrt{\hat{k}^2+\hat{\Omega}}-\lambda\right), \tag{41}$$

and a function representing the capillary effect

$$h(\hat{\Omega},\hat{k}) = -B\hat{k}^2\sqrt{\hat{k}^2+\frac{\alpha_l}{\alpha_s}\hat{\Omega}}\left(\frac{k_s}{k_l}\coth\left(2\lambda\sqrt{\hat{k}^2+\frac{\alpha_l}{\alpha_s}\hat{\Omega}}\right)+1\right). \tag{42}$$

A marginal stability function, $f(\hat{k}) = \hat{\Omega}$, is defined when the dimensionless growth rate is zero. A graph of the marginal stability function

$$f(\hat{k}) = g(0,\hat{k}) + h(0,\hat{k}), \tag{43}$$

illustrates the combined contribution of the thermal and capillary functions to the points of marginal stability, where $f(\hat{k}) = 0$. Fig. 5 shows the behavior of the marginal stability function with respect to the thermal and capillary functions when $\lambda = 0.4$ and $B = 1 \times 10^{-2}$. The curves show that in the longer wavelength region, the marginal stability function is dependent upon the thermal function and shows negligible dependence upon the capillary function. As the wavelengths decrease, the capillary function has a greater influence on the marginal stability function, resulting in a second point of marginal stability in the capillary region. Fig. 5 illustrates that the analytical solution to the dispersion relation when the capillary function is discarded, is a good approximation of the behavior of the growth rate in the longer wavelength regions beyond the point of marginal stability.

Fig. 6 shows the relationship between the analytical and numerical solution for all complex values of the dimensionless growth rate, when $\lambda = 0.4$ and $B = 10^{-2}$. The analytical solution is used to illustrate the behavior of the growth rate in the longer wavelength region. The figure illustrates that the growth rate has an imaginary

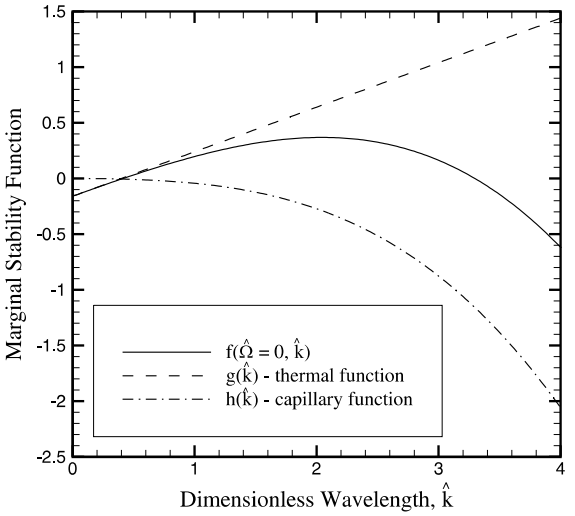

Fig. 5. Marginal stability function at the interface for $\lambda = 0.4$, $B = 10^{-2}$. The points at which $f(0,\hat{k}) = 0$ represent marginal stability at the solid–liquid interface. The contributions to the marginal stability from the thermal gradient, $g(0,\hat{k})$, and the effect of surface curvature, $h(0,\hat{k})$, are also shown.

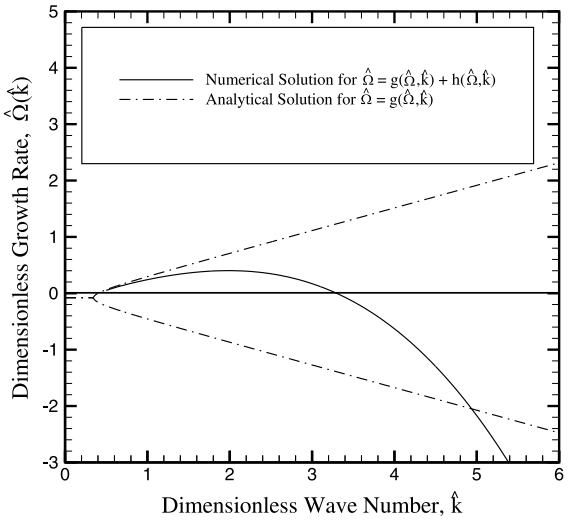

Fig. 6. Real values of the dimensionless growth rate for the numerical and analytical solutions for $\lambda = 0.4$, $B = 10^{-2}$. The function $g(\hat{\Omega},\hat{k})$ represents the thermal gradient while the function $h(\hat{\Omega},\hat{k})$ represents the surface curvature. The numerical solution includes the effects of surface curvature while these are neglected in the analytical solution.

component in the longer wavelength region and that this component, representing a traveling surface wave, is damped or unconditionally stable. Beyond the wave number prescribed in Eq. (37), the growth rate is real and does not have a traveling wave component. This result shows that undamped traveling waves will not occur at the solid–liquid interface. In the analytical solution, the growth has both a positive and negative value beyond the point of marginal stability. The numerical solution begins to deviate from the positive analytical solution in the intermediate wavelength region and reaches a condition of stability in the capillary region. The numerical solution shows that the values for the growth rate in the stable region beyond the point of marginal stability are negative real values.

The relationship between the thermal and capillary functions to the numerical solution of the dispersion relation are shown in Fig. 7 when $\lambda = 0.4$ and $B = 10^{-2}$. The figure illustrates that the value of the thermal function, $g(\hat{\Omega}, \hat{k})$, is positive and increases linearly as the dimensionless wave number approaches infinity. The capillary function is negative and decreases in magnitude following the curve shown in Fig. 7. As the wave number approaches infinity, the capillary function decreases at a faster rate than the value for the thermal function. As a result, the dimensionless wave number is governed by the thermal function in the longer wavelength region, and quickly moves toward the stable regions in the intermediate and capillary regions as the slope of the capillary function continues to increase.

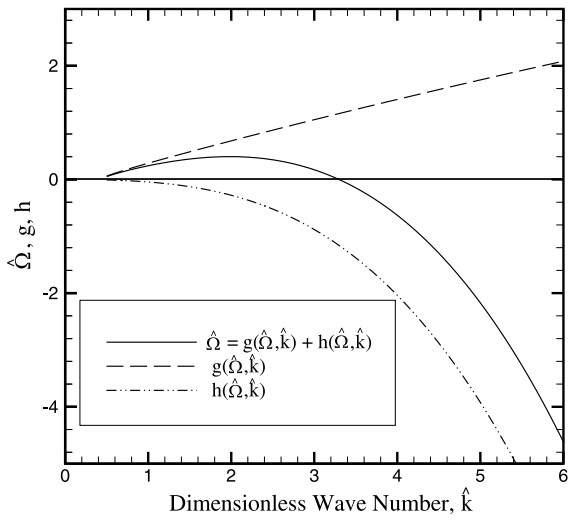

Fig. 7. Numerical solution of the dispersion relation for the growth rate, $\hat{\Omega}$, for $\lambda = 0.4$, $B = 10^{-2}$. The graph shows the contributions of the thermal gradient, $g(\hat{\Omega}, \hat{k})$, and the effect of surface curvature, $h(\hat{\Omega}, \hat{k})$.

Fig. 7 illustrates that if the capillary number is large enough, the magnitude of the linear thermal function will never exceed the nonlinear capillary function leading to a condition of absolute stability where the values of the dimensionless growth rate are negative. The occurrence of absolute stability at the solid–liquid interface was observed in Fig. 4 for increasing values of the capillary number.

If the thermal gradient in the undisturbed liquid is greater than the thermal gradient of the disturbance, the growth rate of the solidifying front will exceed the growth rate of the disturbance. As shown in Fig. 3, the condition of marginal stability in the longer wavelength region illustrates that the growth rate of the solidifying front is larger than the growth rate of the disturbances in the longer wavelength region, and the interface will remain stable. As the wavelengths decrease, the thermal gradient of the disturbance increases linearly and the growth rate of the disturbance exceeds the growth rate of the solidifying front resulting in instability at the solid–liquid interface. The contributions of the thermal gradient in the disturbance are counterbalanced by the effect of the curvature, which has an added effect as the wave number increases. Eventually the interfacial energy is large enough to inhibit growth in the capillary region, and the disturbances are damped.

The undercooling at the solid–liquid interface, given by the Stefan number, can be further analyzed by rewriting Eq. (3) in the following form

$$Ste = Ste_0 + d_0 \frac{\partial^2 s'}{\partial y^2} = Ste_0 - \varepsilon k^2 d_0 e^{i(ky-\omega t)} = \sqrt{\pi}\lambda \operatorname{erfc} \lambda e^{\lambda^2} - B^2 \hat{k}^2 \frac{\varepsilon}{d_0} e^{i(ky-\omega t)} \quad (44)$$

Fig. 2 illustrates the effect of surface curvature on values of the Stefan number when the capillary number, B, is 10^{-2} and the dimensionless wave number, $\hat{k}$, is 30. For these values of the capillary number and wave number, the results from the preceding section predict stable conditions at the solid–liquid interface. In Fig. 2, we assume that the values for the amplitude of the disturbance, ε, and the capillary length, d_0, are of the same order and that the ratio is unity. Fig. 2 shows that for an arbitrary value of the capillary number, undercooling at the interface increases for concave geometry and decreases for convex geometry. At the inflection point, the undercooling at the interface is equal to the background Stefan number, Ste_0. Fig. 2 illustrates that as the solidification parameter approaches infinity, the Stefan number reaches a finite value. Values of the Stefan number that are greater than the finite value are thermally supercooled environments in which the material no longer exists in a supercooled liquid state and solidification occurs instantaneously.

9. Conclusions

A linear perturbation analysis has been applied to a thermally supercooled solidifying front in a half-space. This analysis focuses on instability in an unsteady temperature field for a homogeneous material. A dispersion relation was obtained from solutions to the unsteady energy equations and the boundary condition of heat conservation at the solid–liquid interface.

The results show that the thermal gradients increase the growth rates of disturbances at the solid–liquid interfaces and that the effect of surface curvature results in a decrease in the disturbance growth rates. Further analysis shows that marginal stability occurs in both the longer wavelength and capillary regions. By isolating the terms in the dispersion equation it has been shown that the thermal gradients cause marginal stability in the longer wavelength region. In this region, as the solid–liquid front advances, the growth rate of the solidifying front is larger than the growth rate of the disturbance, and the interface remains planar. As the thermal gradients in the disturbance become larger for increasing wavelengths, the growth rate of the disturbance increases linearly and quickly exceeds the growth rate of the solidifying front. When the effect of surface curvature is included in the dispersion analysis, it is observed that the slope of the capillary function increases while the slope of the thermal function remains constant as the wave number approaches infinity. Greater increases in the capillary function result in a second point of instability in the capillary region, where the growth of the disturbance is not large enough to overcome the interfacial energy at the solid–liquid surface.

References

[1] W.W. Mullins, R.F. Sekerka, Stability of a planar interface during solidification of a dilute binary alloy, J. Appl. Phys. 35 (1964) 444–451.

[2] D.J. Wollkind, L.A. Segel, A nonlinear stability analysis of the freezing of a dilute binary alloy, Philos. Trans. R. Soc. London, Ser. A 268 (1970) 351–380.

[3] M.C. Flemmings, Solidification Processing, McGraw-Hill, New York, 1974, pp. 107–114, 263–289.

[4] W. Kurz, D.J. Fisher, Fundamentals of Solidification, third ed., Trans Tech Publications, Switzerland, 1989, pp. 1–61, 226–237, 293.

[5] R.T. Delves, Theory of interface stability, in: B.R. Pamplin (Ed.), Crystal Growth, Pergamon Press, Oxford, 1975, pp. 40–103.

[6] H.S. Carslaw, J.C. Jaeger, Conduction of Heat in Solids, second ed., Oxford University Press, London, 1959, pp. 282–296.

[7] R.T. Delves, The theory of the stability of the solid–liquid interface under constitutional supercooling (I), Phys. Status Solidi 16 (1966) 621–632.

[8] R.F. Sekerka, Application of the time-dependent theory of interface stability to an isothermal phase transformation, J. Phys. Chem. Solids 28 (1967) 983–994.

[9] S.R. Coriell, G.B. McFadden, R.F. Sekerka, Selection mechanisms for multiple similarity solutions for solidification and melting, J. Cryst. Growth 200 (1999) 276–286.

[10] J. Schaefer, M.E. Glicksman, Creation of dendrites by crystal imperfections, Metall. Trans. 1 (1970) 1973–1978.

[11] K. Oshibata, T. Sato, G. Ohira, Morphological stabilities of planar solid–liquid interfaces during unidirectional solidification of dilute Al–Ti and Al–Cr alloys, J. Cryst. Growth 44 (1978) 419–434.

[12] S.C. Hardy, S.R. Coriell, Morphological stability of ice cylinders in aqueous solution, J. Cryst. Growth 7 (1970) 147–154.

[13] G.B. McFadden, S.R. Coriell, R.F. Sekerka, Analytic solution for a non-axisymmetric isothermal dendrite, J. Cryst. Growth 208 (2000) 726–745.

[14] S.L. Wang, R.F. Sekerka, Computation of the dendritic operating state at large supercoolings by the phase field model, Phys. Rev. E 53 (4) (1996) 3760–3776.

[15] S.C. Sprott, Numerical Recipes, Cambridge University Press, Cambridge, 1991, pp. 254–259.